Mining, Metallurgy & Exploration (2022) 39:1793–1800
https://doi.org/10.1007/s42461-022-00637-6

A Discrete Fracture Network Model for Prediction of Longwall-Induced Permeability

K. M. Ajayi[1] · Z. Khademian[1] · S. J. Schatzel[1] · E. Watkins[1] · V. Gangrade[1]

Received: 13 November 2021 / Accepted: 9 June 2022 / Published online: 17 June 2022

Abstract
Longwall-induced deformations could jeopardize the mechanical integrity of shale gas well casings positioned in the abutment pillar of a longwall mine. The in situ and induced fracture networks surrounding the gas well could provide pathways for gas flow into the mine creating safety concerns. Hence, this study by the National Institute for Occupational Safety and Health (NIOSH) develops a discrete fracture network (DFN) model to characterize the fractures in the overburden based on geomechanical analyses of mining-induced fracture apertures at a study site in southwestern Pennsylvania. The apertures from the geomechanical model are used to develop a stochastic DFN model of the site in fracture flow code (FFC). Multiple realizations of the stochastic DFN model that replicate potential fracture geometries are simulated, and the fracture permeability is compared with field measurements. A maximum field measurement of 5.03×10^{-12} m^2 (5080 mD) and 3.82×10^{-13} m^2 (386 mD) was estimated over the abutment pillar at the Sewickley and Uniontown horizon, respectively. The results show that the average permeabilities from the DFN model agree closely with the field measurements. In addition, the comparison of all the field measurements and 100 DFN realizations show the model is representative of field conditions. These findings provide critical information regarding fracture characteristics in the overburden, which will further be used to predict potential shale gas flow to the mine in the event of a casing breach for an unconventional gas well.

Keywords Shale gas well · Discrete fracture network · Longwall mining

1 Introduction

The recent boom in the shale gas well industry has generated increasing concerns about its impact on safety of underground longwall mining operations in the proximity of the gas wells. Recently, in Pennsylvania, West Virginia, Ohio, Virginia, and Tennessee, shale gas wells have been drilled through current or future longwall mines [1]. This presents a new challenge as longwall-induced deformations could jeopardize the mechanical integrity of the shale gas well casing, which creates safety concerns for the mines [1]. With the recent increase in deep cover mining and the application of longwall mining methods for coal extraction, an update is required to the 1957 Pennsylvania gas well pillar recommendations, which were for room-and-pillar mining under shallow cover [2]. In 2012, the Pennsylvania Department of Environmental Protection (PADEP) initiated a call for research to update the gas well pillar regulation. Consequently, researchers from the National Institute for Occupational Safety and Health (NIOSH) have been evaluating the impact of longwall-induced deformation on gas well stability under shallow and deep cover with the objective of providing recommendations for pillar design to avoid casing failure. Findings from this project identified three main horizons for potential casing failure: the overlying coal/weak seams (highlighted in Fig. 1), 0–10 m (0–32.8 ft) below the mine floor and 0–30 m (0–98.4 m) above the mine roof [2]. Similarly, there is risk of failure(s) if the distance between the gas well casing and the edge of the gob (L_1 and L_2 in Fig. 1) is within 50 ft, because the gas well might be affected by the pillar yield and peak abutment pressure zone [3]. Figure 1 shows a schematic elevation view of the two adjacent panels with a shale gas well located over the abutment pillar at a study site in the Pittsburgh coal bed. The mining depth varies across these locations in southwestern Pennsylvania, and Marcellus shale depth could vary from 1500 to 2700 m [2].

✉ K. M. Ajayi
ony2@cdc.gov

[1] Centers for Disease Control and Prevention, National Institute for Occupational Safety and Health, Pittsburgh, PA, USA

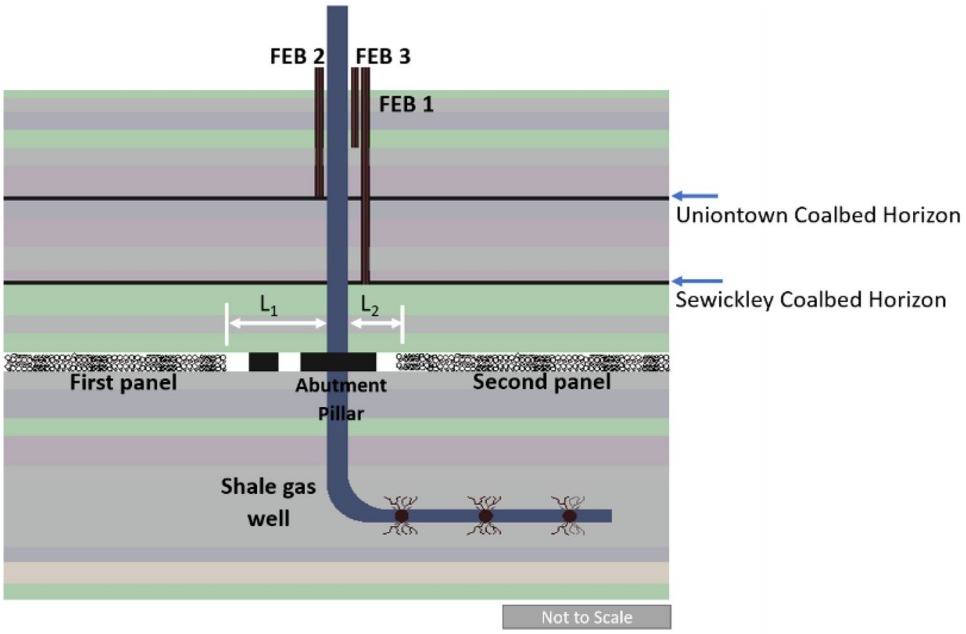

Fig. 1 Schematic of shale gas well through the abutment pillar of a longwall mine. L_1 and L_2 are the distance of the first and second panel from the gas well casing, respectively

In the event of a breach, gas from the casing (with production pressure up to 2.41 MPa or more) could flow through the path of least resistance into the mine, increasing the risk of an explosion as methane accumulates beyond the mandated concentrations. Therefore, it is necessary to study potential flow of shale gas into the mine and provide proactive measures for the safety of mine workers. This requires knowledge of the permeability of each stratum in the overburden, especially from the failure location to the mine roof. Permeability changes due to mining-induced deformation, with a hundred or thousands millidarcy increase during undermining. This could continue to change up to 7 months after mining [4]. These changes could be estimated using field studies, numerical modeling, or a combination of both methods. This study combines both methods by developing a stochastic DFN model based on core log data from a site in southwestern Pennsylvania to predict mining-induced permeability changes.

Prior to this numerical modeling effort, three boreholes (shown in Fig. 1: FEB1, FEB2, and FEB3) were drilled over the abutment pillar at the study site to monitor permeability changes during the mining of two longwall panels. In addition to these three boreholes, a fourth borehole was drilled to monitor the horizontal displacement of strata during mining. The surface subsidence measurement data are compared with the results of the geomechanical model developed for the test site in 3DEC considering in situ and mining-induced stresses. The code 3DEC, a three-dimensional distinct element code by Itasca [5], is used for geomechanical analyses of the mining-induced fracture aperture variations. With a reasonable agreement established between the geomechanical model and the field subsidence data, the fracture parameters for each stratum in the overburden are obtained from 3DEC. Based on these fracture parameters, an independent DFN model is developed using a code developed by the authors (fracture flow code—FFC). FFC is developed to generate a stochastic fracture network based on the site data, predict permeability at any specified location, and solve for gas flow through the fracture network. It is used to generate multiple realizations of the fracture network in the overburden and determine the permeability over the abutment pillar. The overburden is classified as the caved zone, fractured zone, and bending zone [6], and the fractured zone is characterized by rock blocks (or rock matrix), vertical (or near vertical) fractures, and horizontal fractures at the bedding planes (or interfaces between the rock layers) [7]. The fracture permeabilities from the models are compared with the field measurements at the measured horizons. The DFN fracture permeabilities are determined from the surface down to the top of the fractured zone with 50 layers identified in the overburden. Since the field measurements focused on the region above the abutment pillar, this study focuses on fracture permeability for each stratum in the overburden.

2 Research Approach

2.1 Site Geology and Field Study

The study was conducted in the northern Appalachian Basin with a site mining the Pittsburgh coal bed using the longwall mining method. The deformation and induced fracturing in the associated stratigraphy of the Pittsburgh formation, upper Pennsylvanian system, due to mining are important

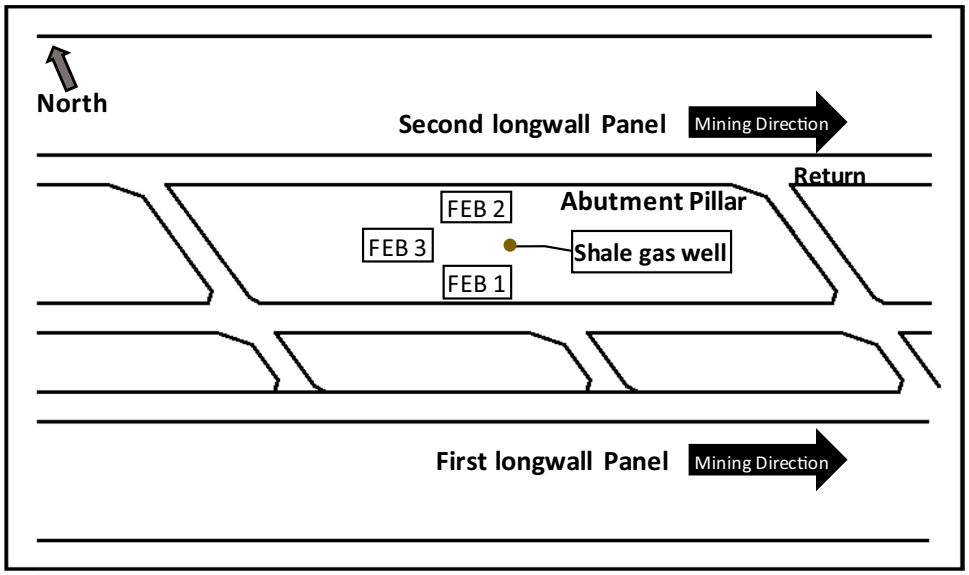

Fig. 2 Layout of longwall mine site

to the integrity of wells in the abutment pillars. Three boreholes (FEB 1, FEB 2, and FEB 3) were drilled at the test site to monitor permeability changes at three horizons during and after undermining. The overburden depth considered is 146.9 m (482 ft) with multiple weak to strong rock interfaces and a longwall panel width of 457.2 m (1500 ft). Figure 2 shows the plan view of the site with two longwall panels, location of the three permeability measurement boreholes, three-entry gate-road system, and a 38.1 m × 83.82 m (125 ft × 275 ft) abutment pillar. FEB 1 monitored a 124.97-m (410 ft) depth, which targets the Sewickley coal horizon; FEB 2 monitored a 79.29-m (260 ft) depth, which targets the Uniontown coal horizon; and FEB 3 monitored the 41.15-m (135 ft) depth, which targets the projected top of the fractured zone.

The stratigraphic data collected during the field study are shown in Fig. 3 from 83.2-m (273 ft) depth to the mine roof with the projected Sewickley horizon. The rock types in the overburden are shale, sandstone, sandy shale, limestone, coal, and shaley limestone. The seam height is about 1.83 m (6 ft), so the caved zone is assumed to be 10.7 m (35 ft), which is within the acceptable range of 4 to 6 times the mining height. This implies that the 9.45-m (31 ft) thick shale and 0.91-m (3 ft) sandy shale directly above the seam formed the caved zone. Hence, the fractured zone starts at 35 ft above the mine corresponding to a depth of 443 ft (135.03 m). During this process, which spanned over a year, permeability measurements were conducted during undermining; the first panel was mined before the second panel. For each horizon, the field experiments conducted falling-head slug testing to estimate mine-induced permeability; detailed methodology of the field study is published by [8], and the results are summarized in Table 1. The results show that mining induces significant permeability variation

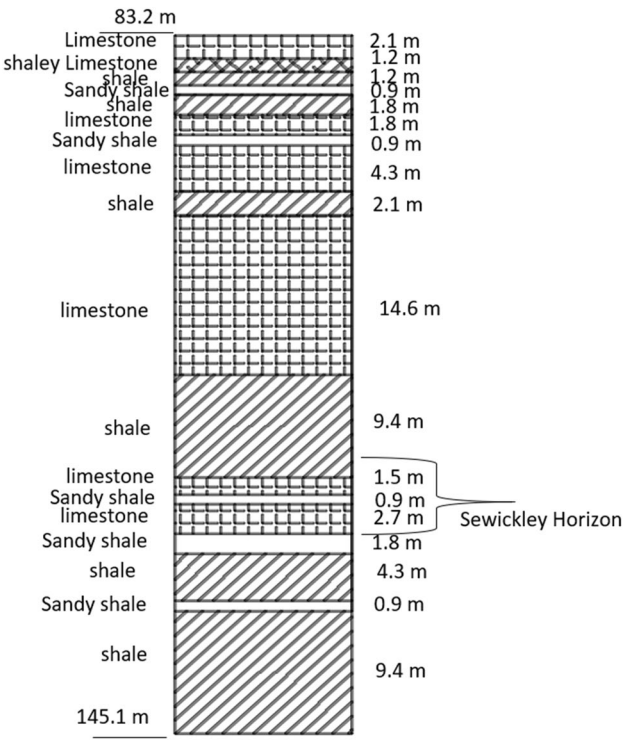

Fig. 3 Lithological description of the rock units from 83.2 m (273 ft) to the mine

Table 1 Summary of field permeability measurements

Borehole ID	First panel (mD)		Second panel (mD)	
	Min	Max	Min	Max
FEB 1	4.11×10^{2}	1.36×10^{3}	1.1×10^{3}	5.08×10^{3}
FEB 2	2.19×10^{1}	2.45×10^{2}	1.15×10^{1}	3.86×10^{2}
FEB 3	2.73×10^{3}	3.29×10^{4}	3.85×10^{4}	1.32×10^{5}

in the overburden, and the maximum permeability value was measured while undermining the second panel due to the combined impact of both panels mining.

2.2 Geomechanical Study

Flow rate through fractures is related to the fracture hydraulic aperture (b), which is defined as the physical distance between fracture plates, and fracture roughness. A pseudo-2D model is constructed in 3DEC with a unit length in the out-of-plane direction. The DFN method is used for generating near-vertical fractures, and interfaces are used for separating geological strata. Figure 4 shows the central part of the model has a three-entry longwall gate-road system of 18 m × 38 m centers. The model length is extended from left and right boundaries to reach a length of 9000 m (29,528 ft) in total, avoiding boundary effects on the longwall-induced deformation. The DFN fracture density and friction are calibrated against surface subsidence data measured after mining the first and then the second panel. Using the calibrated model, b is estimated from an initial aperture value, and the fracture deformation induced from stress analyses is given as follows:

$$b = b_0 + F \triangle u \quad (1)$$

where F is a correction factor relating to the fracture roughness and flow tortuosity, b_0 is the initial value of hydraulic aperture (mm), and Δu is the fracture deformation after applying mechanical stresses (mm). In a geomechanical model, Δu can be calculated through the relationship between stress, displacement, and constitutive laws, but b_0 and F are unknown variables and depend on the fracture slip history and intrinsic roughness. This paper assumes fractures have smooth surfaces, and thus, F is the unit, and b_0 is estimated as 0.5 mm through a calibration process using pre-mining permeability values measured in the field. After the second panel is mined and the model reaches equilibrium, the aperture values along each fracture in the model are exported to FFC for permeability estimation.

2.3 DFN Permeability Model and Parameters

The field permeability measurements were obtained over the abutment pillar, and only three horizons were targeted in the overburden. However, this study focuses on determining the permeability for each stratum in the overburden, specifically the fractured zone. The horizontal fractures are modeled as interfaces between different lithologies, and the near-vertical fractures are modeled stochastically. From the site core log data, 50 layers are modeled with thickness greater than 0.6 m, and the model height is 135.3 m based on the distance from the surface (continuous zone) to the top of the caved zone.

The locations of the fracture centers are modeled with uniform distribution, and the fracture trace lengths (L_t) are modeled using power law distribution. The orientations of the near-vertical fractures are modeled with von Mises-Fisher's distribution with a variance of 20° from 65- to 135.3-m depth and 10° from surface (0 m) to 64.9-m depth. The fracture density is modeled by developing a function based on a previous field study in Tahmoor Colliery (New South Wales, Australia) [9]. The aperture distribution for this study is modeled using log-normal distribution with peak values assigned based on results from the geomechanical model. The code (FFC) is developed such that the bedding plane and fractures in each bed are first generated. Thereafter, the corresponding fracture backbone for each layer, which represents the connected fractures, is developed, and fractures with no connectivity are eliminated. Figure 5 shows the fracture network for both panels; the thicker lines indicate the region over the gob area of the fractured zone, which decreases towards the surface based on a rib angle of 8°. For this study, the permeability is determined over the abutment pillar close to the second panel as indicated in Fig. 5.

2.4 Numerical Model for Permeability

The vertical and horizontal permeabilities are determined based on the method described in previous studies [10]. Flow

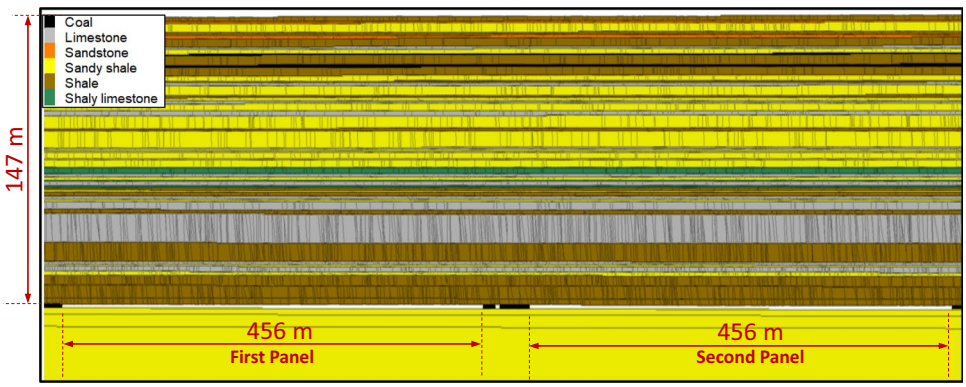

Fig. 4 Central part of a two-panel model of a longwall mine simulated in 3DEC

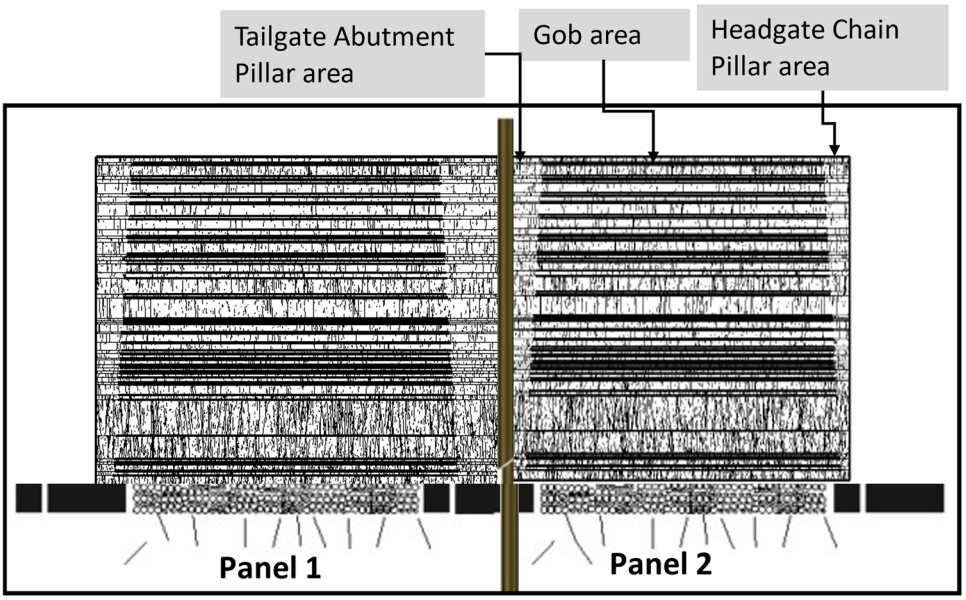

Fig. 5 Fracture network for the site including the first and second panel

through the fractures is modeled using the cubic law, and the permeabilities are determined using Darcy's equation:

$$\begin{bmatrix} q_{xx} & q_{xy} \\ q_{yx} & q_{yy} \end{bmatrix} = \begin{bmatrix} K_{xx} & K_{xy} \\ K_{yx} & K_{yy} \end{bmatrix} \begin{bmatrix} \nabla H_x & 0 \\ 0 & \nabla H_y \end{bmatrix} \quad (2)$$

where q indicates the direction of flow and velocity (m/s), and it is calculated by dividing the sum of boundary flow from cubic law (Q) by the boundary area. ∇H_x and ∇H_y are the pressure head gradients in the x and y directions respectively, and K is the permeability coefficient or conductivity (m/s). A boundary pressure is applied independently in both directions to obtain the principal (q_{yy} and q_{xx}) and cross flow (q_{xy} and q_{yx}) in the y and x directions, respectively (Fig. 6). The corresponding intrinsic or absolute permeability tensor (k in m^2), which is a property of the porous media, is calculated from the following:

$$k = \frac{K\mu}{\rho g} \quad (3)$$

ρ is the density of fluid kg/m^3, g is the acceleration due to gravity (m/s^2), and μ is the dynamic viscosity of the fluid (Ns/m^2). The principal absolute permeabilities in the x (k_{xx}) and y (k_{yy}) directions are the horizontal and vertical permeability.

Similar to the field study, a hydrostatic pressure head is applied independently to establish the pressure head gradient required to determine the horizontal and vertical permeability. The bedding planes are assumed to be laterally extensive, and the fracture length is assumed to be the effective flow path with negligible convolutedness to ignore tortuosity effects. Apertures could vary across a fracture length, but a uniform aperture is assumed for each fracture. The aperture is the hydraulic or effective aperture, which represents the aperture that will produce the same flow rate as a rough-walled fracture under the same pressure gradient. The DFN model (in Fig. 5) is generated using FFC, and the permeability is calculated for each of the 50 layers. Also, 100 realizations are generated for this stochastic model to account for variability in the fracture geometry.

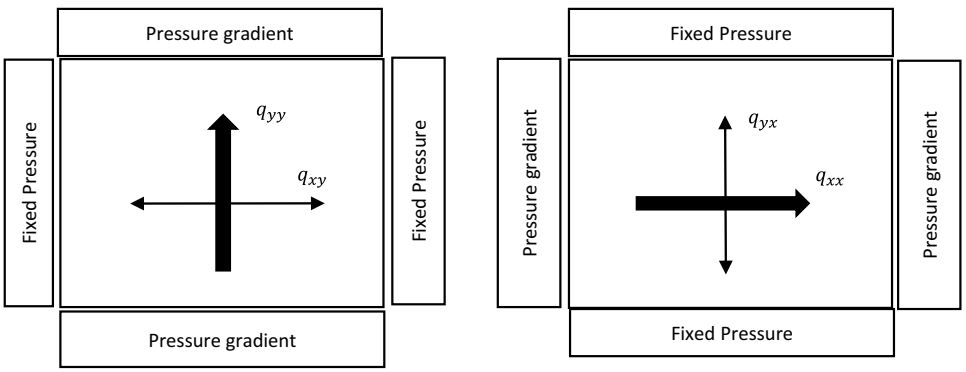

Fig. 6 Boundary condition for determining permeability

3 Results and Discussion

The results presented in this study focus on the prediction of permeability after mining of the second panel, since it was estimated to have the highest permeability from the field study in Table 1. The fracture aperture predicted from the geomechanical analyses in 3DEC is related to the in situ and longwall-induced stresses as discussed in Section 2.2. Figure 7 shows the aperture of the horizontal (Fig. 8a) and near-vertical (Fig. 8b) fractures over the abutment pillar after mining the second panel. Aperture values above 1 mm in Fig. 7 are mostly related to the fractures above the panel edge where a high concentration of shear and tensile stresses activates nearby fractures and enhances their aperture values. The lower values of aperture are associated with the DFNs above the pillars and at the center of the panels. This can be related to the high compression originating from the horizontal stresses that further close the fractures and reduce their aperture values. In Fig. 8a, the aperture values above 1 mm are mostly associated with the bedding plane separation at the panel edges and the caved zone. The lower range of aperture values in Fig. 7a is related to the high vertical compression from the overburden loads mostly concentrated above the pillars and the region above the gob at the center of panels. These results are used to determine the peak value for the log-normal distribution used to characterize fracture aperture for each stratum from surface to the mine roof as shown in Fig. 7a and b for near horizontal and vertical fractures, respectively.

As discussed, 100 DFN realizations are used to model different fracture geometries to determine permeability. Figure 8 shows the ensembled permeability average over the abutment pillar for each layer after mining the second panel along with the maximum field measurements obtained at three main horizons of interest. Figure 9 shows the complete results of the 100 DFN realizations at the Sewickley horizon. The results show a significant variation in the permeabilities from the surface to top of the caved zone. For the horizontal permeabilities (in Fig. 8a), most of the values are within the

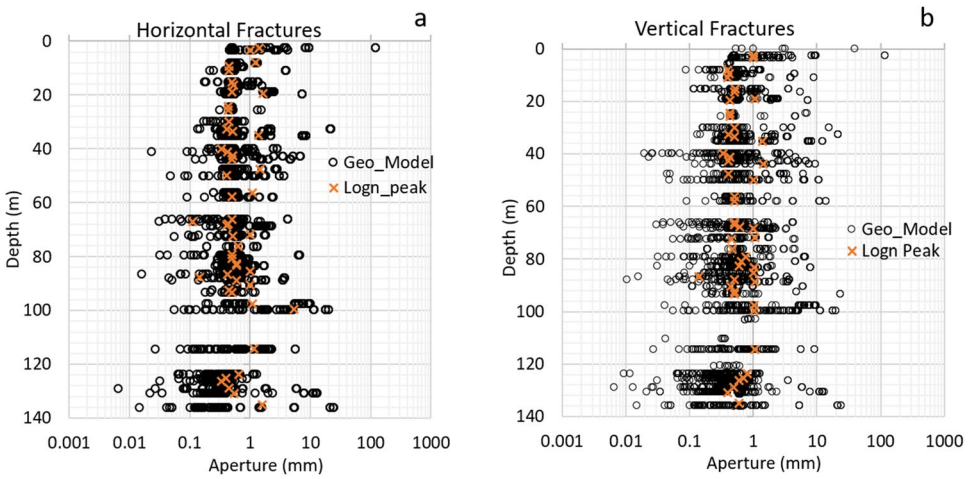

Fig. 7 Aperture of fractures over the abutment pillar after mining the second panel and peak of lognormal distribution for **a** horizontal fractures and **b** vertical fractures

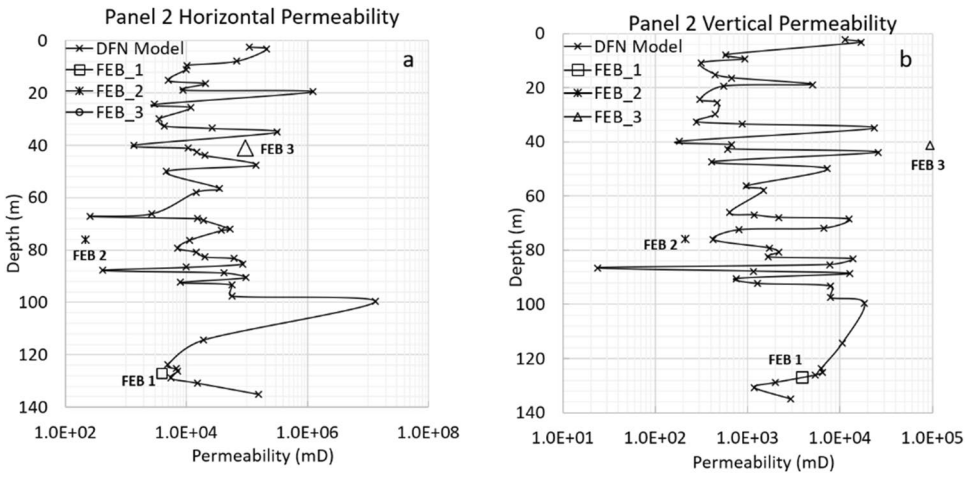

Fig. 8 Plot of permeability variation with depth after the mining of the second panel. **a** Horizontal permeability and **b** vertical permeability

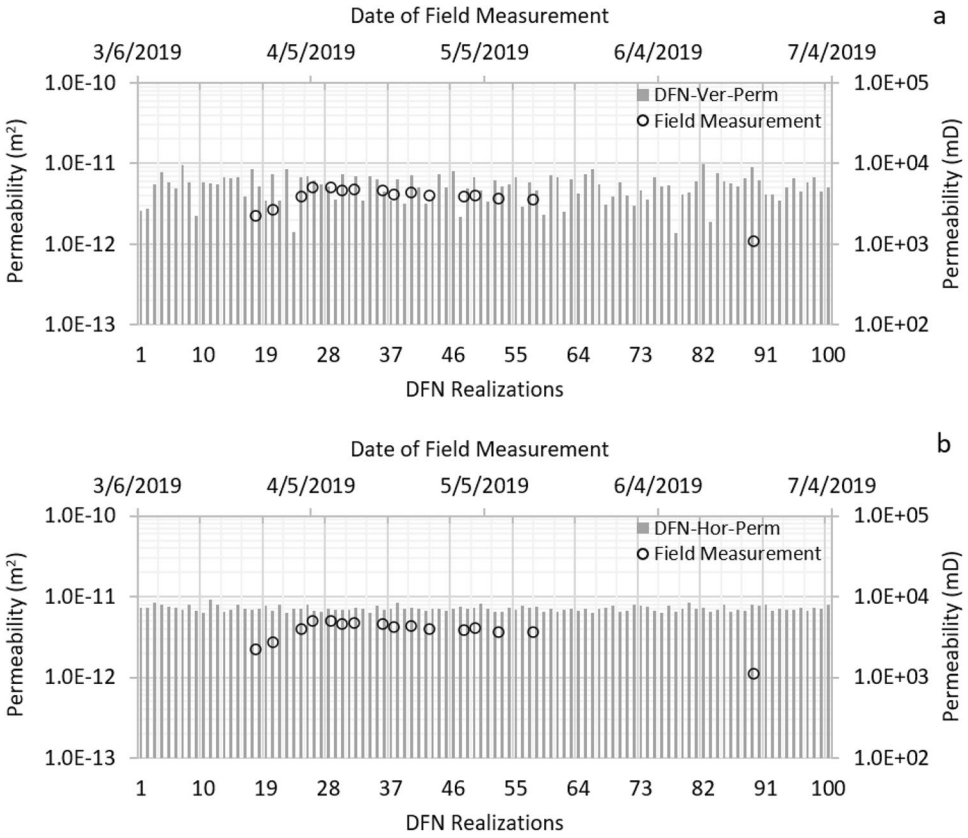

Fig. 9 Permeability at the Sewickley horizon during second panel mining. Comparison of field permeability measurements with results from 100 DFN realizations for **a** vertical permeability and **b** horizontal permeabilities

same order of magnitude. However, there are specific horizons that have notably higher permeabilities compared to the nearby strata. This is due to large bed separations at these horizons, which could potentially be linked to the impact of a bridge layer discussed by Palchik [6].

Both the vertical and horizontal permeabilities show a higher permeability range towards the surface due to the impact of mining-induced deformations and subsidence. These average permeabilities are within close orders of magnitude as the maximum measured permeability; however, the vertical permeabilities are closer to the field measurements. The field measurements were obtained by conducting the falling-head slug test to estimate the resultant permeability, which is representative of both permeabilities. As the water is added to the borehole, the slotted casing at the test horizon facilitates the application of pressure in both directions. Consequently, the field data from borehole experiments are interpreted to represent both vertical and horizontal permeabilities. As observed in Fig. 8, the horizontal permeabilities after mining are higher than the vertical permeabilities for each of the stratum due to large bed separation. This agrees with previous findings that the subvertical (bedding perpendicular) permeability tends to be much lower than the subhorizontal (bedding parallel) permeability due to mining-related bed separations [11]. Between the two horizontal fractures that embed each layer (above and below), the vertical fractures that transport flow between both horizontal fractures could potentially have less impact on the horizontal permeabilities. Hence, the horizontal permeability is mainly dependent on the aperture of fractures defined between the interfaces, which varies due to the response of each stratum to the mining-induced deformation.

The vertical permeability, as shown in Fig. 8b, varies from the surface to the mining horizon and could be dependent on parameters such as the fracture density, aperture sizes, and connectivity. For the thick layers, there are possibilities that some of the fractures in the stratum might not connect to both horizontal fractures creating dead ends. Consequently, some realizations could have lower vertical permeability, mostly when the vertical fractures are not connected through the stratum. For the projected Sewickley horizon, Fig. 9 shows the complete 100 realization results for the vertical and horizontal permeabilities over the abutment pillar along with the data obtained from the field study for the projected Sewickley horizon. Both the horizontal and vertical permeabilities are within the same order of magnitude as the field measurements obtained from March 26 to June 20, 2019. The results indicate that the apertures predicted from the geomechanical studies are representative of the mine condition specifically over the abutment pillar. Based on this agreement, it is assumed that the fracture characterization from the geomechanical model could be used to define the

properties of the other locations where field measurements were not conducted, specifically for fractures over the gob region.

4 Conclusions

A stochastic DFN model is developed based on the site core log data to predict the horizontal and vertical permeabilities from the surface to the top of the caved zone. One-hundred DFN realizations are generated to determine the vertical and horizontal permeabilities for the isolated zone over an abutment pillar after the mining of the second panel. The results show that the vertical and horizontal permeabilities from the DFN model compare closely with field measurements, which indicates that the resultant permeability obtained from the field measurements is representative of both permeabilities. It also shows that the fracture data from the geomechanical model are representative of the field conditions with validation using the ground movement data obtained from the site and the permeability results in this study. With this agreement, the aperture data for other zones of the mine could be obtained from the geomechanical model—specifically, for the fractured zone over the gob. Based on the successful validation of this DFN model, this model could be further developed to predict the permeability of the fractured zone over the gob with fracture aperture obtained from the geomechanical analysis. This will complete the fracture characterization of the overburden, which could be used to predict potential shale gas flow to the mine in the event of a breach. This prediction could provide information on the associated risk of a casing breach and determination of appropriate guideline to proactively prevent such occurrence.

Acknowledgements The authors acknowledge the contributions of Dr. C. Özgen Karacan during the review of the modeling approach. Data from this manuscript had been presented at the North American Mine Ventilation Symposium, June 2021, Rapid City, SD [12].

Declarations

Conflict of Interest The authors declare no competing interests.

Disclaimer The findings and conclusions in this paper are those of the authors and do not necessarily represent the official position of the National Institute for Occupational Safety and Health, Centers for Disease Control and Prevention. Mention of any company or product does not constitute endorsement by NIOSH.

References

1. Su DW, Zhang P, Van Dyke M, Minoski T (2019) Effect of longwall-induced subsurface deformations on shale gas well casing stability under deep covers. Int J Min Sci Technol 29(1):3–8
2. Zhang P, Su D, Lu J (2019) Influence of longwall mining on the stability of shale gas wells in barrier pillars. in American Rock Mechanics Association. New York
3. Zhang P, Dougherty H, Su D, Trackemas J (2019) Influence of longwall mining on the stability of gas wells in chain pillars. in Proceedings of the 38th International Conference on Ground Control in Mining
4. Schatzel SJ, Karacan CÖ, Dougherty H, Goodman GV (2012) An analysis of reservoir conditions and responses in longwall panel overburden during mining and its effect on gob gas well performance. Eng Geol 127:65–74
5. Itasca U (2013) 3DEC—3 dimensional distinct element code. Itasca Consulting Group Inc., Minneapolis
6. Palchik V (2005) Localization of mining-induced horizontal fractures along rock layer interfaces in overburden: field measurements and prediction. Environ Geol 48(1):68–80
7. Palchik V (2003) Formation of fractured zones in overburden due to longwall mining. Environ Geol 44(1):28–38
8. Watkins E, GV, Schatzel S, Hollerich C, Addis J (2020) Permeability determination for potential interaction between shale gas wells and the coal mine environment due to longwall-induced deformations., in 2020 SME Annual Meeting and Exhibit. Phoenix, AZ
9. Holla L, Buizen M (1991) The ground movement, strata fracturing and changes in permeability due to deep longwall mining. Int J Rock Mech Min Sci Geomech Abstr. Elsevier
10. Zhang X, Sanderson D, Harkness R, Last N (1996) Evaluation of the 2-D permeability tensor for fractured rock masses. Int J Rock Mech Min Sci Geomech Abstr. Elsevier
11. Heller R, Vermylen J, Zoback M (2014) Experimental investigation of matrix permeability of gas shalesexperimental investigation of matrix permeability of gas shales. AAPG bulletin 98(5):975–995
12. Ajayi K, Khademian Z, Schatzel S, Watkins E, Gangrade V (2021) Numerical modeling of longwallinducedpermeability under shallow cover, in mine Ventilation. CRC Press pp 389–397